

# AERODYNAMIC SHAPE OPTIMIZATION OF HYPERSONIC AIRLINERS CONSIDERING MULTI-DESIGN-POINT

Atsushi UENO\*, Hideyuki TAGUCHI\*, Kojiro SUZUKI\*\*  
 \*Japan Aerospace Exploration Agency, \*\*The University of Tokyo

**Keywords:** *Hypersonic, Transonic, Subsonic, Optimization*

## Abstract

*A hypersonic airliner experiences a wide range of Mach numbers, which requires the multi-design point optimization of the aerodynamic shape to maximize the aircraft performance such as the flying range. Our research objective is to propose a design guide of the aerodynamic shape for hypersonic airliners by conducting an aerodynamic shape optimization based on Computational Fluid Dynamics (CFD) with the consideration of three design points (i.e., take-off, transonic flight, and hypersonic cruise). Results show that the improvement in both the subsonic lift coefficient and the transonic lift-to-drag ratio ( $L/D$ ) can be achieved, though it degrades the hypersonic  $L/D$ . The lower surface of the rear part of the vehicle should be convex upward to increase the transonic  $L/D$ , whereas, it should be nearly flat or slightly convex downward to increase the hypersonic  $L/D$ . This conflicting design requirement results in the trade-off between the transonic and hypersonic  $L/D$ s. The shape of the lower surface of the vehicle is the key design factor to obtain a well-balanced aerodynamic performance covering a wide range of Mach numbers.*

## 1 Introduction

Research projects to develop hypersonic airliners are conducted in Europe [1] and Japan [2]. For the development of commercially successful hypersonic transports, the hypersonic lift-to-drag ratio ( $L/D$ ) is one of the most important parameters because it strongly affects the flying range. The transonic  $L/D$  should also be taken into account because a small transonic  $L/D$  demands large engines to break the sound

barrier. In addition to  $L/D$ s, a large lift coefficient at low-subsonic speed is required to obtain a sufficient take-off performance using existing airports. Consequently, a well-balanced aerodynamic performance covering a wide range of Mach numbers from low-subsonic speed to hypersonic speed should be achieved. However, hypersonic airliners tend to have a small-aspect-ratio wing due to a large sweep-back angle, which makes it difficult to improve the subsonic and transonic aerodynamic performances. Our research objective is to propose a design guide of the aerodynamic shape for hypersonic airliners that can achieve a well-balanced aerodynamic performance from low-subsonic speed to hypersonic speed. For this purpose, a Computational Fluid Dynamics (CFD) based aerodynamic shape optimization was conducted with the consideration of three design points (i.e., take-off, transonic flight, and hypersonic cruise). In the optimization study, the planform shape was fixed due to strict design requirements, and only the cross-section shape was optimized.

First, the reference shape was defined based on a conventional design approach. Then the aerodynamic shape was optimized in two steps. In the first step, only the hypersonic  $L/D$  was optimized to maximize the cruise efficiency. In the second step, all the design points were taken into account. Finally, a design guide is concluded.

## 2 Definition of Reference Shape

We assumed a hypersonic airliner of a similar size to the Concorde supersonic airliner (Fig. 1). Major design requirements for the wing are: (a) the wing area and thickness should be large to

improve the fuel (liquid hydrogen) tank volume, (b) the wing with large thickness should have a subsonic leading edge to reduce the wave drag at the hypersonic cruise, (c) the aspect ratio of the wing should be large to increase the transonic and subsonic  $L/Ds$ , and (d) the shock cone generated at the nose should not impinge on the wing. Based on these requirements, the double-delta planform was adopted to the wing. The inner wing has a large wing thickness and large wing area to house a fuel tank in it and also has a subsonic leading edge (at Mach 5) to reduce the wave drag. The outer wing has a supersonic leading edge to improve the subsonic and transonic  $L/Ds$  and also has a small wing thickness to reduce the wave drag. The wing span was defined by the compromise between design requirements (c) and (d). Here, the degree of freedom of the planform design is low due to these design requirements. For this reason, the planform shape was fixed and only the cross-section shape was optimized in this study.

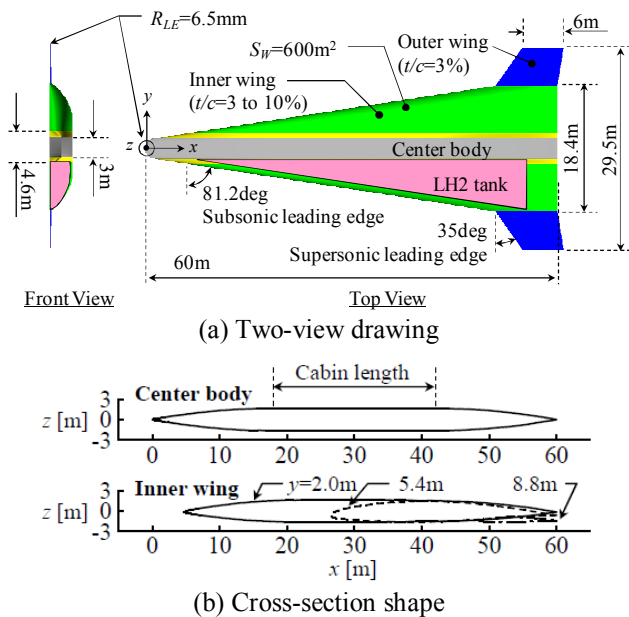


Fig. 1. Reference shape of hypersonic airliner

The aerodynamic heating rate at the leading edge was calculated by using an empirical relation for a cylinder [3]. The leading edge radius at the supersonic leading edge was set to 6.5mm so that the radiation equilibrium temperature at the leading edge becomes 1,200K at the hypersonic cruise condition (i.e.,

Mach 5 at an altitude of 90,000ft). In the calculation of the radiation equilibrium temperature, the emissivity was set to 0.8.

The cross-section shape of the center body at  $y=0m$  is shown in Fig. 1(b), and was composed of two tangent ogives and a rectangle that represents the cabin (at  $x=18m$  to  $42m$ ). To satisfy the constraint of the aerodynamic heating, the leading edge of the front tangent ogive was rounded to a value of  $R_{LE}=6.5mm$ . The cross-section shape is similar at any section of the center body. The cross-section shapes of the inner wing were based on the NACA 6-series airfoil, which has been used for many supersonic vehicles. At the section from  $y=1.5m$  to  $y=2.3m$  (the area shown in yellow in Fig. 1), the cross-section shape was defined by the interpolation between that of the center body at  $y=1.5m$  and that of the inner wing at  $y=2.3m$ . The thickness-to-chord ratio ( $t/c$ ) of the inner wing varied from 3 to 10% along the spanwise direction. The large  $t/c$  is due to the demand for a large fuel tank volume. The cross-section shape of the outer wing at the wing-tip section was based on the NACA 64A-203 airfoil, with the leading edge radius modified to 6.5mm. To reduce the wave drag, the  $t/c$  of the outer wing was set to 3%. The cross-section shape is similar at any section of the outer wing. To produce a large hypersonic lift and to provide proper mounting for the nacelle under the inner wing, the lower surface of the inner wing was almost flat, though the nacelle was not considered in the CFD analysis.

### 3 Method of Optimization

The aerodynamic shape optimization was conducted by using a 3D Euler CFD flow solver and the Sequential Quadratic Programming (SQP) method [4], [5] as an optimizer.

In the flow analysis, the symmetric TVD scheme [6] was used to discretize the convective term and the Matrix-Free Gauss-Seidel method [7] was used for the implicit time integration. The lift and pressure drag coefficients ( $C_L$  and  $C_{D,p}$ , respectively) were obtained from the Euler analysis. The skin friction drag coefficient ( $C_{D,f}$ ) was calculated by using an empirical relation based on the turbulent skin friction coefficient

over a flat plate and accounting for the effect of compressibility [8]. Aerodynamic coefficients are referenced to the wing area (i.e., 600m<sup>2</sup>). The grid topology was C-H type (i.e., C-type in the chordwise direction and H-type in the spanwise direction). The number of grid points was 281 in the chordwise direction, 71 in the spanwise direction, and 60 in the normal direction to the surface in the subsonic and transonic analyses, and 281, 61, and 46 in the corresponding directions in the hypersonic analysis. The grid for the hypersonic analysis is shown in Fig. 2. For the subsonic and transonic analyses, the far field boundary was 15 times the body length away from the vehicle.

The nonlinear constrained optimization problem was solved by applying the SQP method. The Broyden-Fletcher-Goldfarb-Shanno approximation [9] was applied to the second derivative of the objective function in the Quadratic Programming problem.

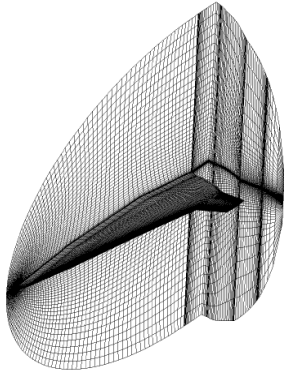


Fig. 2. Grid for hypersonic analysis

#### 4 Definition of Optimization Problem

The reference shape, which was the initial shape in the optimization study, was approximated by the Bezier curves and the Bezier surfaces. Positions of their control points shown in Fig. 3 and Table 1 were selected as design variables to be optimized. In Fig. 3, only the upper surface is shown. The surface geometry is shown on the starboard side and control points are shown on the portside. The cross-section shape of the center body was defined at  $y=0m$  by two Bezier curves and line. The cross-section shape is similar at any section of the center body. The inner wing was defined by the Bezier surface.

The cross-section shape in the area shown in yellow in Figs. 1 and 3 was defined by the interpolation as described in section 2. The cross-section shape of the outer wing was defined at the wing tip section by the Bezier curve. The cross-section shape is similar at any section of the outer wing.

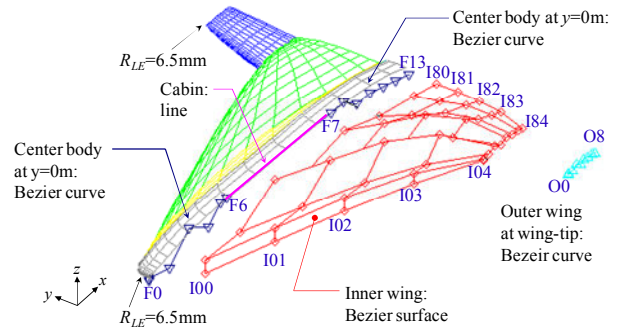


Fig. 3. Definition of aerodynamic shape using Bezier curves and Bezier surfaces

Table 1. Design variables

1	z	F	0	U	25	z	I	1	0	L	53	z	I	1	1	L	81	z	I	1	2	L	109	z	I	1	3	L
2	z	F	2	U	26	z	I	2	0	L	54	z	I	2	1	L	82	z	I	2	2	L	110	z	I	2	3	L
3	z	F	3	U	27	z	I	3	0	L	55	z	I	3	1	L	83	z	I	3	2	L	111	z	I	3	3	L
4	z	F	4	U	28	z	I	4	0	L	56	z	I	4	1	L	84	z	I	4	2	L	112	z	I	4	3	L
5	z	F	2	L	29	z	I	5	0	L	57	z	I	5	1	L	85	z	I	5	2	L	113	z	I	5	3	L
6	z	F	3	L	30	z	I	6	0	L	58	z	I	6	1	L	86	z	I	6	2	L	114	z	I	6	3	L
7	z	F	4	L	31	z	I	7	0	L	59	z	I	7	1	L	87	z	I	7	2	L	115	z	I	7	3	L
8	z	F	9	U	32	y	I	2	1	U	60	y	I	2	2	U	88	y	I	2	3	U	116	z	O	2	U	
9	z	F	10	U	33	y	I	3	1	U	61	y	I	3	2	U	89	y	I	3	3	U	117	z	O	3	U	
10	z	F	11	U	34	y	I	4	1	U	62	y	I	4	2	U	90	y	I	4	3	U	118	z	O	4	U	
11	z	F	12	U	35	y	I	5	1	U	63	y	I	5	2	U	91	y	I	5	3	U	119	z	O	5	U	
12	z	F	13	U	36	y	I	6	1	U	64	y	I	6	2	U	92	y	I	6	3	U	120	z	O	6	U	
13	z	F	9	L	37	y	I	7	1	U	65	y	I	7	2	U	93	y	I	7	3	U	121	z	O	7	U	
14	z	F	10	L	38	y	I	8	1	U	66	y	I	8	2	U	94	y	I	8	3	U	122	z	O	2	L	
15	z	F	11	L	39	z	I	0	1	U	67	z	I	0	2	U	95	z	I	0	3	L	123	z	O	3	L	
16	z	F	12	L	40	z	I	1	1	U	68	z	I	1	2	U	96	z	I	1	3	L	124	z	O	4	L	
17	z	I	0	0	U	41	z	I	2	1	U	69	z	I	2	2	U	97	z	I	2	3	L	125	z	O	5	L
18	z	I	1	0	U	42	z	I	3	1	U	70	z	I	3	2	U	98	z	I	3	3	L	126	z	O	6	L
19	z	I	2	0	U	43	z	I	4	1	U	71	z	I	4	2	U	99	z	I	4	3	L	127	z	O	7	L
20	z	I	3	0	U	44	z	I	5	1	U	72	z	I	5	2	U	100	z	I	5	3	L					
21	z	I	4	0	U	45	z	I	6	1	U	73	z	I	6	2	U	101	z	I	6	3	L	128	Transonic			
22	z	I	5	0	U	46	z	I	7	1	U	74	z	I	7	2	U	102	z	I	7	3	L	AoA				
23	z	I	6	0	U	47	y	I	2	1	L	75	y	I	2	2	L	103	y	I	2	3	L					
24	z	I	7	0	U	48	y	I	3	1	L	76	y	I	3	2	L	104	y	I	3	3	L					
						49	y	I	4	1	L	77	y	I	4	2	L	105	y	I	4	3	L					
						50	y	I	5	1	L	78	y	I	5	2	L	106	y	I	5	3	L					
						51	y	I	6	1	L	79	y	I	6	2	L	107	y	I	6	3	L					
						52	y	I	7	1	L	80	y	I	7	2	L	108	y	I	7	3	L					

The design variables, which consist of 127 coordinate values of control points and the transonic angle of attack, are listed in Table 1. In this table, 'y' and 'z' in the first column correspond to y and z coordinate values, respectively. The second column ('F', 'I', and 'O') coupled with the third column (e.g., '70') specifies control points shown in Fig. 3. In the final column, 'U' and 'L' indicate upper and lower surfaces, respectively.

Table 2 summarizes the optimization problem considering three design points. The hypersonic  $L/D$  was maximized under the constraints of the aerodynamic performance and shape. At transonic speed, the  $L/D$  was constrained at multiple-value ( $G1$ ) to obtain the trade-off between the hypersonic and transonic  $L/D$ s. The hypersonic and transonic lift coefficients should be sufficient to sustain a straight and level flight ( $G2$  and  $G3$ ). At low-subsonic speed, the lift coefficient should be larger than 0.44 ( $G4$ ) to achieve an appropriate take-off performance using existing airports. Regarding the aerodynamic shape, the leading edge radius ( $G5$ ), the fuel tank volume ( $G6$ ), and the wing thickness ( $G7$  and  $G8$ ) were constrained.

Table 2. Optimization problem

Design variables	Positions of control points (see Table 1) Transonic angle of attack <sup>*1)</sup>		
Objective	Hypersonic <sup>*2)</sup> $L/D$	Maximized	
Constraint	$G1$	Transonic <sup>*3)</sup> $L/D$	= multiple-value
	$G2$	Hypersonic $C_L$	= 0.075
	$G3$	Transonic $C_L$	= 0.12
	$G4$	Subsonic <sup>*4)</sup> $C_L$	$\geq 0.44$
	$G5$	Leading edge radius of center body and outer wing	= 6.5mm
	$G6$	Fuel tank volume	= 700m <sup>3</sup>
	$G7$	Outer-wing thickness	$\geq 3\%c$ ( $x=40\%c$ )
	$G8$	Inner-wing thickness	$\geq 0.5\%c$ ( $x=95\%c$ )

\*1) The hypersonic and subsonic angle of attacks were fixed at 5° and 10°, respectively.

\*2) Mach number is 5 and flight altitude is 90,000ft.

\*3) Mach number is 1.05 and flight altitude is 30,000ft.

\*4) Mach number is 0.3 and flight altitude is 0ft.

## 5 Results and Discussion

### 5.1 Optimization of hypersonic $L/D$

In this section, the hypersonic  $L/D$  was maximized without constraint functions of the subsonic and transonic aerodynamic performances (i.e.,  $G1$ ,  $G3$ , and  $G4$ ). Based on the results, the design guide of the aerodynamic shape required to maximize the cruise efficiency is discussed.

Table 3 shows the results of the optimized shape (referred to as Case A) and the reference

shape that is the initial shape in the optimization study. The comparison of the aerodynamic coefficients between these two shapes is summarized in Table 4. Figure 4 shows the surface pressure contour plots. The  $C_L$  of the reference shape is smaller than the constraint value (Table 3). In this study, the hypersonic angle of attack was constrained to be less than 5° considering the passengers' comfort. Therefore, the aerodynamic shape should be modified to increase the  $C_L$  as well as to decrease the  $C_D$  to maximize the  $L/D$ .

Table 3. Optimization results  
(design Mach number: 5)

	Reference	Case A
Hypersonic $L/D$	4.91	5.60
Hypersonic $C_L$	0.069	0.075
Leading edge radius	6.5mm	6.5mm
Fuel tank volume	689m <sup>3</sup>	700m <sup>3</sup>
Outer-wing thickness @ $x=40\%c$	3.0% $c$	3.0% $c$
Inner-wing thickness @ $x=95\%c$	0.8% $c$	1.1% $c$

Table 4. Comparison of aerodynamic coefficient  
(Mach 5, AoA=5°)

Reference	$C_L$	$C_{D,p}$	$C_{D,f}$	$L/D$
Center body	0.0141	0.0030	0.0005	4.08
Inner wing	0.0448	0.0071	0.0015	5.17
Outer wing	0.0102	0.0017	0.0002	5.23
Total	0.0692	0.0118	0.0023	4.91

Case A	$C_L$	$C_{D,p}$	$C_{D,f}$	$L/D$
Center body	0.0148	0.0024	0.0005	5.05
Inner wing	0.0484	0.0071	0.0015	5.63
Outer wing	0.0118	0.0017	0.0002	6.29
Total	0.0750	0.0112	0.0022	5.60

The cross-section shapes of the front and rear parts of the center body change from a tangent ogive to a nearly straight shape (Fig. 5(a)). As a result, the compression of the flow becomes weak on the lower surface, which decreases the lift coefficient. At the rear part of the center body, the  $z$ -coordinate value of the trailing edge of the optimum shape is smaller than that of the reference shape (Fig. 5(a)). Then the expansion of the flow over the upper surface increases, whereas that over the lower surface decreases. As a result, the lift coefficient

increases at the rear part of the center body, which compensates for the decrease in the lift coefficient at the front part of the center body (Table 4). The drag coefficient is decreased due to the thin front part of the center body, which weakens the shock wave. As a result, the  $L/D$  of the center body is increased from 4.08 to 5.05.

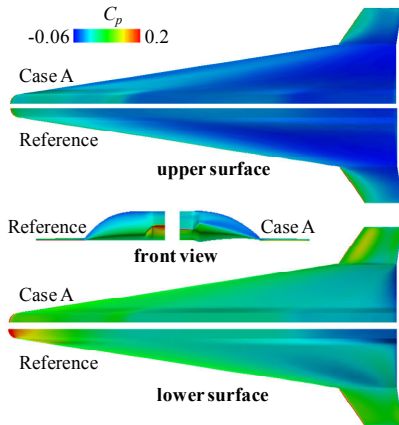


Fig. 4. Pressure contour plots (Mach 5, AoA=5°)

The shape changes in the lower surface and the leading edge of the inner wing realize the increase in the  $C_L$ . The lower surface of the optimum shape is slightly convex downward and the curvature of the optimum shape on the lower surface is smaller than that of the reference shape (Figs. 5(b) and 5(c)). The expansion of the flow over the lower surface is suppressed due to these changes in the shape, which leads to the increase in the  $C_L$ . The upper surface of the optimum shape near the leading edge has a larger curvature that makes the flow expand more rapidly to increase the  $C_L$ , though the decrease in the  $C_L$  is found at the downstream of the flow expansion on the upper surface. Due to these two shape changes, the  $C_L$  of the inner wing is increased (Table 4). The  $C_D$  of the inner wing is not increased as a result of the optimization, whereas the  $C_L$  is increased. The important parameters for this fact are the wing thickness and the shape of the lower surface. At outboard wing sections (e.g., at  $y=5.9\text{m}$ , Fig. 5(c)), the wing thickness becomes small, which leads to the decrease in the  $C_D$  as well as the decrease in the fuel tank volume. However, the fuel tank volume is increased to satisfy the constraint function  $G6$  (Table 3). The

increase in the fuel tank volume is realized at inboard wing sections (e.g., at  $y=2.9\text{m}$ , Fig. 5(b)) due to the shape of the lower surface near the trailing edge that is slightly convex downward, while the wing thickness, which strongly affects the  $C_D$ , is similar between the optimum and reference shapes. As seen above, the wing thickness at outboard wing sections and the shape of the lower surface are important to the drag reduction as well as the improvement in the fuel tank volume.

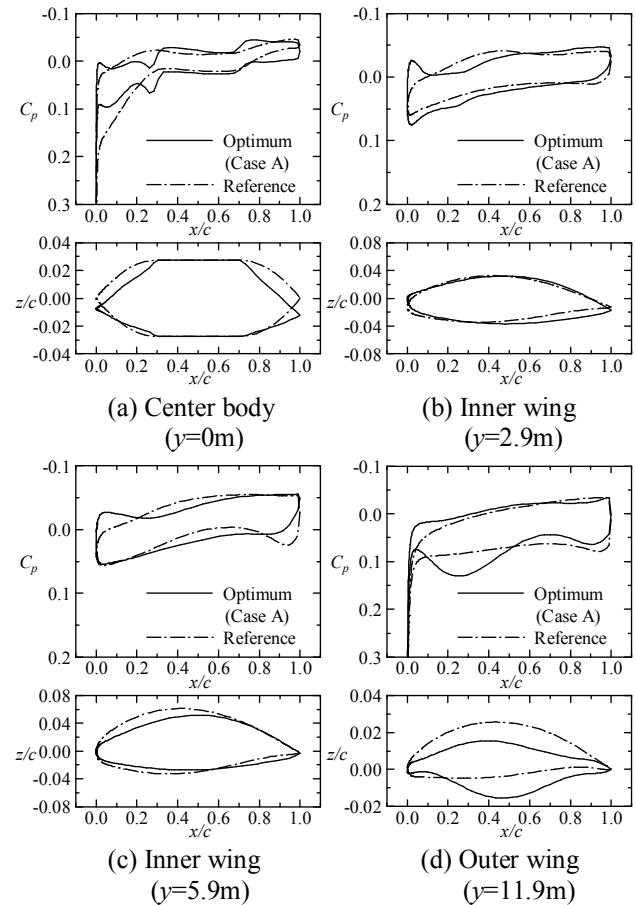


Fig. 5. Cross-section shapes and  $C_p$  distributions (Mach 5, AoA=5°)

The increase in the lift coefficient of the outer wing is realized by two types of modification to the shape: (a) the maximum  $z$ -coordinate value of the upper surface of the optimum shape is smaller than that of the reference shape (Fig. 5(d)), making the flow over the upper surface expand more strongly, which decreases the pressure coefficient, and (b) the minimum  $z$ -coordinate value of the lower surface of the optimum shape is also smaller

than that of the reference shape (Fig. 5(d)), which increases the pressure coefficient due to the compression caused by the larger frontal projected area. As a result, the lift coefficient increases from 0.0102 to 0.0118 (Table 4). The drag reduction is also realized by a shape change. To decrease the hypersonic pressure drag, which is much larger than the skin friction drag, the thickness of the optimum shape near the leading edge is decreased from the reference shape (Fig. 5(d)), whereas the leading edge radius is the same (i.e., 6.5mm). Decreasing the leading-edge thickness causes the bow shock wave near the leading edge to weaken and the pressure coefficient to decrease, which decreases the pressure drag coefficient.

The cross-section shapes and the pressure contour plots on the planes normal to the  $x$ -axis are shown in Fig. 6. The center body and the inner wing of the optimum shape are blended more smoothly and the lower surface is nearly flat especially at the rear part of the vehicle. The nearly flat surface compresses the flow efficiently, which contributes to the increase in the  $C_L$ .

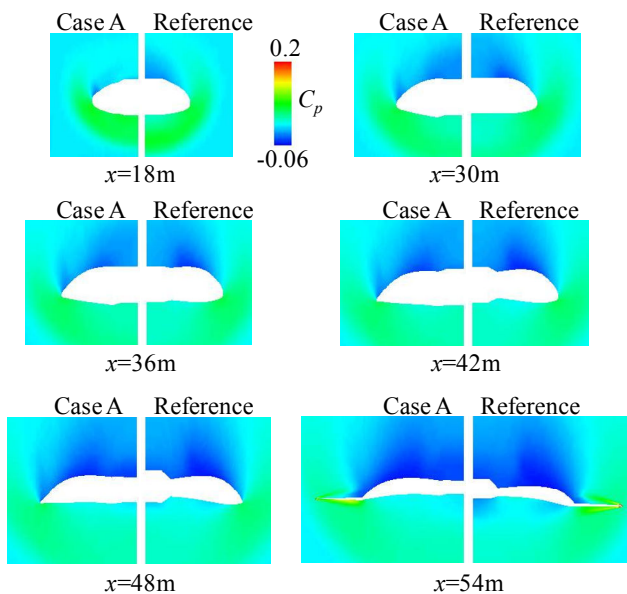


Fig. 6. Cross-section shapes normal to  $x$ -axis (Mach 5,  $AoA=5^\circ$ )

Based on the results discussed above, the key design guides to improve the hypersonic  $L/D$  are summarized as follows: (a) the radius of the supersonic leading edge should be small to decrease the  $C_D$  as long as the constraint of the

aerodynamic heating is satisfied, (b) the lower surface of the outer wing with a supersonic leading edge should be convex downward to increase the  $C_L$ , and (c) the lower surface of the inner wing with a subsonic leading edge should be nearly flat or slightly convex downward to increase the  $C_L$  and the fuel tank volume.

## 5.2 Optimization with three design points

In this section, the optimization problem with three design points shown in Table 2 was solved. In the optimization study, the constraint value of the transonic  $L/D$  ( $GI$ ) was set to 6, 7, and 7.5. The aerodynamic performances of optimum shapes are shown in Fig. 7. In this figure, Case B and Case C are the optimum shapes in the case of  $GI=6$  and 7, respectively. When the constraint value of  $GI$  is 7.5, this constraint was not satisfied. Case D corresponds to the optimum shape that achieves the maximum transonic  $L/D$ .

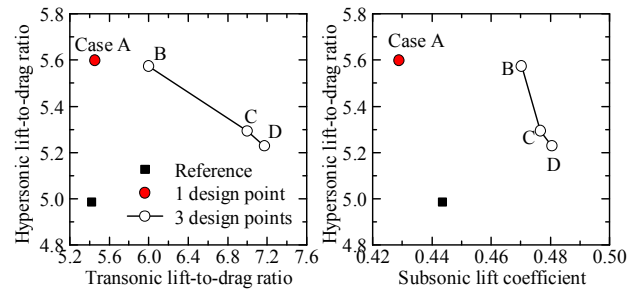


Fig. 7. Aerodynamic performances of optimum shapes at each design point

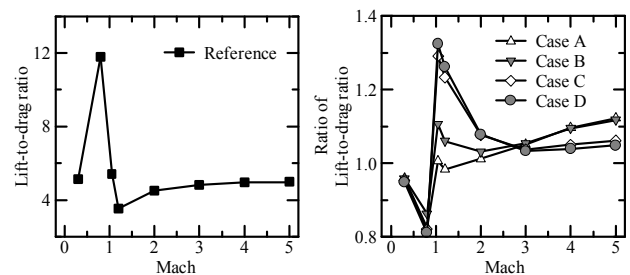


Fig. 8. Lift-to-drag ratio of optimum shapes

Figure 8 shows the  $L/D$ s of the optimum shapes. The  $L/D$ s are evaluated at the  $C_L$  required to sustain a straight and level flight at each Mach number. The right figure in Fig. 8 shows the ratio of the  $L/D$ s of the optimum shapes to that of the reference shape.

The results of Cases A and B show that it is possible to improve the transonic  $L/D$  with the hypersonic  $L/D$  kept at nearly same level. However, larger improvement in the transonic  $L/D$  causes the degradation of the hypersonic  $L/D$  (e.g., compared with Cases A and C, the transonic  $L/D$  was improved by about 28%, whereas the hypersonic  $L/D$  was degraded by about 5%). The subsonic  $C_L$  was improved by about 14% in Cases B, C, and D compared to that of Case A in which the subsonic and transonic aerodynamic performances were not considered. However, the results of Cases B, C, and D show that the compromise in the hypersonic  $L/D$  contributes to only a small increase in the subsonic  $C_L$ . Thus, the trade-off between the transonic and hypersonic  $L/D$ s is important to achieve a well-balanced aerodynamic performance covering a wide range of Mach numbers. Based on these facts, the design guide of the aerodynamic shape is discussed comparing the results of Cases A and C from the viewpoint of the transonic and hypersonic  $L/D$ s.

The pressure contour plots of Cases A and C at transonic speed are shown in Fig. 9. The difference in the pressure distribution can be seen in the vicinity of the trailing edge. In fact, the pressure on both upper and lower surfaces of Case C is higher than that of Case A in this area. The apparent difference in the aerodynamic shape can be seen at the leading edge of the inner wing, that is, the bluntness of the inner wing is larger in Case C. The cross-section shapes and  $C_p$  distributions at transonic speed are shown in Fig. 10. Table 5 shows the comparison of the aerodynamic coefficients at each design point.

The largest improvement in the transonic  $L/D$  is realized at the outer wing (Table 5). The transonic angle of attack in Case C ( $0.3^\circ$ ) is smaller than that in Case A ( $1.1^\circ$ ), which reduces the lift at the front part of the outer wing in Case C (Fig. 10(d)). On the other hand, the rear part of the outer wing produces larger lift in Case C due to the shape of the lower surface. The curvature at the crest of the lower surface (i.e., at  $x/c=0.45$ ) is smaller in Case C (Fig. 10(d)), which reduces the expansion of the flow at the downstream of the crest. Then the

flow is compressed because the lower surface at the rear part of the outer wing is convex upward. As a result, the  $C_D$  is decreased and the  $C_L$  is almost the same even though the angle of attack is smaller, which leads to the improvement in the transonic  $L/D$  by 98% (Table 5). The hypersonic  $L/D$  of the outer wing is decreased by only 1.6%, though the transonic  $L/D$  is largely improved. The wing thickness of the outer wing is 3% both in Cases A and C due to the constraint function  $G7$ , and therefore, the frontal projected area, which strongly affects the hypersonic  $L/D$ , is the same. Consequently, at the outer wing with the supersonic leading edge, the transonic  $L/D$  can be improved with the hypersonic  $L/D$  kept at nearly same level.

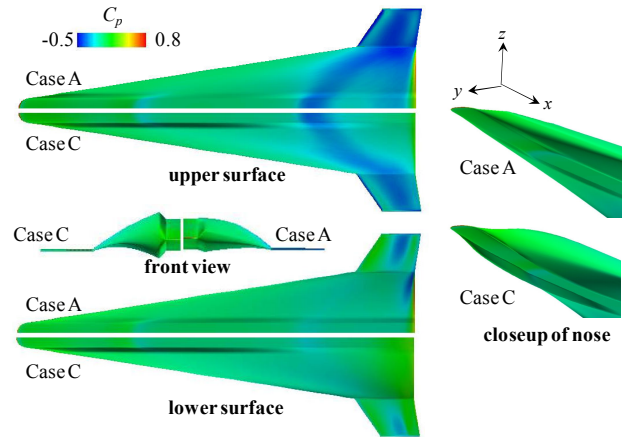


Fig. 9. Pressure contour plots  
(Mach 1.05, AoA= $1.1^\circ$ (Case A),  $0.3^\circ$ (Case C))

Table 5. Comparison of aerodynamic coefficient

	Mach 0.3		Mach 1.05		Mach 5.0	
	$C_L$	$L/D$	$C_L$	$L/D$	$C_L$	$L/D$
Case A						
Center body	0.055	3.6	0.014	2.8	0.015	5.1
Inner wing	0.257	4.9	0.071	4.8	0.048	5.6
Outer wing	0.116	6.1	0.035	16.8	0.012	6.3
Total	0.429	4.9	0.120	5.5	0.075	5.6

	Mach 0.3		Mach 1.05		Mach 5.0	
	$C_L$	$L/D$	$C_L$	$L/D$	$C_L$	$L/D$
Case C						
Center body	0.062	3.7	0.014	2.9	0.015	4.8
Inner wing	0.294	4.9	0.074	6.4	0.048	5.3
Outer wing	0.121	6.1	0.032	33.2	0.011	6.2
Total	0.477	4.9	0.120	7.0	0.075	5.3

The differences in the shape of the center body are as follows: (a) the bluntness of the

nose on the upper surface is larger in Case C, and (b) at the rear part of the center body in Case C, the upper surface is convex downward and the lower surface is convex upward (Fig. 10(a)). The former modification to the shape produces the transonic lift, however, it decreases the hypersonic  $L/D$  due to the stronger shock wave in front of the nose. The latter compresses the flow both on the upper and lower surfaces at transonic speed, which results in the decrease in the transonic  $C_D$ . At the center body, the transonic  $L/D$  can be improved, whereas the hypersonic  $L/D$  is reduced mainly by the nose bluntness.

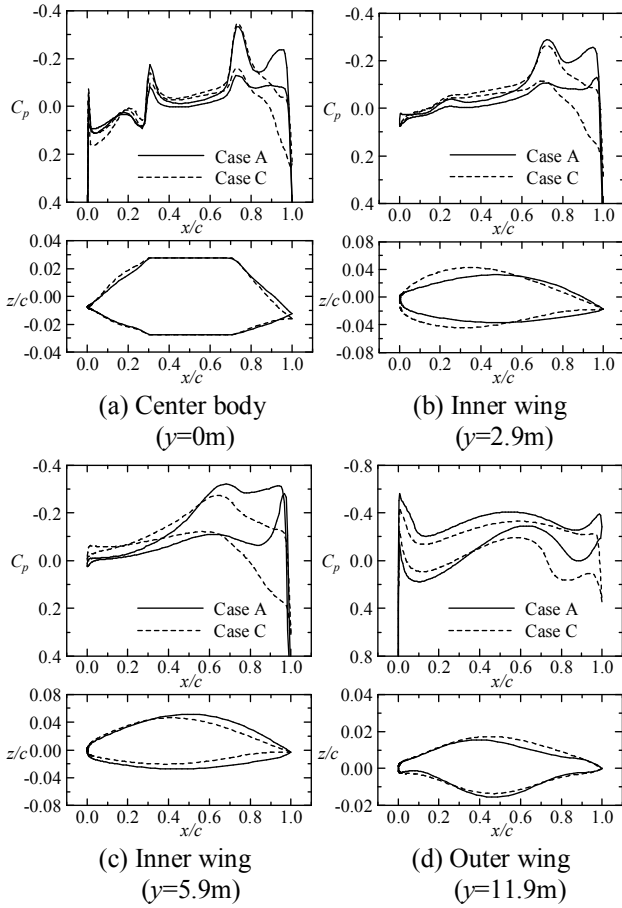


Fig. 10. Cross-section shapes and  $C_p$  distributions (Mach 1.05, AoA=1.1°(Case A), 0.3°(Case C))

The shape modification to the inner wing is the same as that to the center body. The rear part of the inner wing in Case C improves the transonic  $L/D$  in the same way as the center body discussed above (Figs. 10(b) and 10(c)). However, this shape modification to the rear

part of the inner wing causes the decrease in the fuel tank volume in this region. To satisfy the constraint of the fuel tank volume, the leading edge bluntness becomes larger in Case C. The large bluntness contributes to the improvement in the transonic  $L/D$  as well as the decrease in the hypersonic  $L/D$  at the center body. In contrast, it does not improve the transonic  $L/D$  due to the large sweep-back angle and causes only the hypersonic drag. At the inner wing as well as the center body, the improvement in the transonic  $L/D$  degrades the hypersonic  $L/D$ .

The subsonic  $C_L$  is increased at the rear part of the vehicle due to the shape modification needed to improve the transonic  $L/D$  (Fig. 11). Thus, the subsonic  $C_L$ , which is larger than the constraint value in Case C (Table 5), and the transonic  $L/D$  can be improved at the same time.

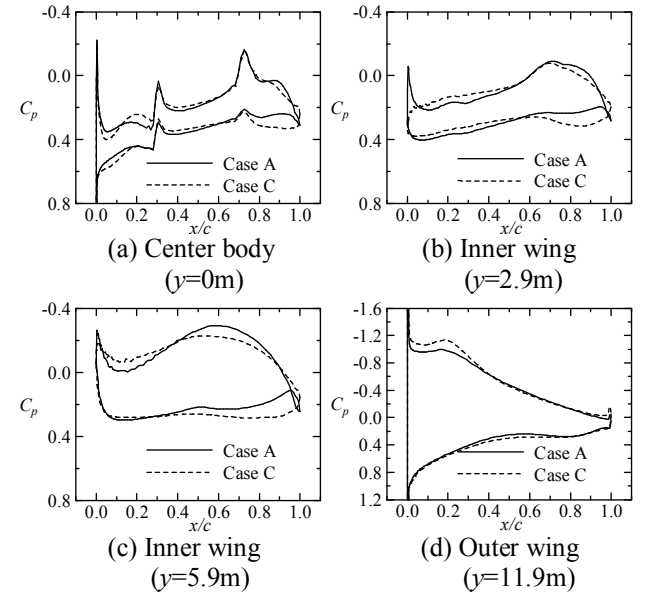


Fig. 11. Cross-section shapes and  $C_p$  distributions (Mach 0.3, AoA=10°)

## 6 Conclusion

The cross-section shape of a hypersonic airliner was optimized by using the CFD analysis and the SQP method as an optimizer. In the optimization study, three design points (i.e., take-off, transonic flight, and hypersonic cruise) were considered. The aerodynamic heating (the radius of the supersonic leading edge), the fuel tank volume, and the planform shape were fixed during the optimization. Results show that the subsonic  $C_L$  and the transonic  $L/D$  can be

improved at the same time, whereas there is a trade-off between the transonic and the hypersonic  $L/D$ s. To improve the hypersonic  $L/D$ , the following is noted. (a) The radius of the supersonic leading edge should be small as long as the constraint of the aerodynamic heating is satisfied. (b) The lower surface should be nearly flat along the spanwise direction and slightly convex downward along the flow direction. On the other hand, to improve the transonic  $L/D$ , the upper and lower surfaces at the rear part of the vehicle should be convex downward and upward, respectively. This conflicting requirement to the shape design of the lower surface results in the trade-off between the transonic and hypersonic  $L/D$ s. Thus, the shape of the lower surface of the vehicle is the key design factor to obtain a well-balanced aerodynamic performance covering a wide range of Mach numbers.

- [9] Fletcher R. A New Approach to Variable Metric Algorithms. *Computer Journal*, Vol. 13, pp 317-322, 1970.

### Copyright Statement

The authors confirm that they, and/or their company or organization, hold copyright on all of the original material included in this paper. The authors also confirm that they have obtained permission, from the copyright holder of any third party material included in this paper, to publish it as part of their paper. The authors confirm that they give permission, or have obtained permission from the copyright holder of this paper, for the publication and distribution of this paper as part of the ICAS2010 proceedings or as individual off-prints from the proceedings.

### References

- [1] Steelant J. Sustained Hypersonic Flight in Europe: Technology Drivers for LAPCAT II. *16th AIAA/DLR/DGLR International Space Planes and Hypersonic Systems and Technologies Conference*, Bremen, AIAA 2009-7240, 2009.
- [2] Taguchi H, Murakami A, Sato T and Tsuchiya T. Conceptual Study on Hypersonic Airplanes using Pre-Cooled Turbojet. *15th AIAA International Space Planes and Hypersonic Systems and Technologies Conference*, Dayton, Ohio, AIAA 2008-2503, 2008.
- [3] Tauber M. E., Bowles J.V. and Yang L. Use of Atmospheric Braking During Mars Missions. *Journal of Spacecraft and Rockets*, Vol. 27, No. 5, pp. 514-521, 1990.
- [4] Fletcher R. *Practical Methods of Optimization*. John Wiley and Sons, 1987.
- [5] Powell M. J. D. *Variable Metric Methods for Constrained Optimization, Mathematical Programming: The State of the Art*. (A. Bachem, M. Grotschel and B. Korte, eds.), Springer Verlag, 1983.
- [6] Yee H. C. A class of high-resolution explicit and implicit shock-capturing methods. NASA TM 101088, 1989.
- [7] Shima E. A Simple Scheme for Structured/Unstructured CFD. *Proceedings of the 29th Fluid Dynamics Conference*, pp 325-328, 1997. (in Japanese)
- [8] Raymer D. P. *Aircraft Design: A Conceptual Approach*. 4th edition, AIAA Education Series, AIAA, 2006.